Addition of H$_2$O and O$_2$ to Acetone and Dimethylsulfoxide Ligated Uranyl(V) Dioxocations

Christopher M. Leavitt,[†] Vyacheslav S. Bryantsev,[‡] Wibe A. de Jong,[§] Mamadou S. Diallo,[‡] William A. Goddard III,[‡] Gary S. Groenewold,*,[||] and Michael J. Van Stipdonk*,[†]

Department of Chemistry, Wichita State University, Wichita, KS, Materials and Process Simulation Centre, Beckman Institute 139-74, California Institute of Technology, Pasadena, CA, William R. Wiley Environmental Molecular Sciences Laboratory, Pacific Northwest National Laboratory, Richland, WA, and Interfacial Chemistry Group, Idaho National Laboratory, Idaho Falls, ID

Gas-phase complexes of the formula [UO$_2$(lig)]$^+$ (lig = acetone (aco) or dimethylsulfoxide (dmso)) were generated by electrospray ionization (ESI) and studied by tandem ion-trap mass spectrometry to determine the general effect of ligand charge donation on the reactivity of UO$_2^+$ with respect to water and dioxygen. The original hypothesis that addition of O$_2$ is enhanced by strong σ-donor ligands bound to UO$_2^+$ is supported by results from competitive collision-induced dissociation (CID) experiments, which show near exclusive loss of H$_2$O from [UO$_2$(dmso)(H$_2$O)(O$_2$)]$^+$, whereas both H$_2$O and O$_2$ are eliminated from the corresponding [UO$_2$(aco)(H$_2$O)(O$_2$)]$^+$ species. Ligand-addition reaction rates were investigated by monitoring precursor and product ion intensities as a function of ion storage time in the ion-trap mass spectrometer: these experiments suggest that the association of dioxygen to the UO$_2^+$ complex is enhanced when the more basic dmso ligand was coordinated to the metal complex. Conversely, addition of H$_2$O is favored for the analogous complex ion that contains an aco ligand. Experimental rate measurements are supported by density function theory calculations of relative energies, which show stronger bonds between UO$_2^+$ and O$_2$ when dmso is the coordinating ligand, whereas bonds to H$_2$O are stronger for the aco complex.

Introduction

Uranium−oxygen species and their intrinsic reactivity are of interest because of their importance to the nuclear energy industry and because their chemistry is fundamental to our understanding of the migration and fate of uranium in the environment and to the development of efficient and effective methods for separation from fission products and other actinides.[1−5] Speciation of uranium is diverse, and includes multiple oxidation states, oxide forms, and multiuranium clusters: each species can exhibit variable reactivity, stability, and solubility.[6,7]

Fundamental reactions between uranium and (molecular) O$_2$ have been investigated in the gas and condensed phases. For example, it was shown that gas-phase U$^+$ reacts with O$_2$ to yield UO$^+$; this cation reacts with a second O$_2$ molecule to form the reduced uranyl cation UO$_2^+$, formally a U(V) species.[8] A similar reaction of U^{2+} with O$_2$ and other oxidants yielded the (doubly charged) UO^{2+} and the UO$_2^{2+}$ cations.[9,10] In the condensed phase, O$_2$ addition to uranyl centers generally occurs to furnish η^2-peroxo species, and there are examples of materials in which uranyl molecules (UO$_2^{2+}$) are bridged by peroxide in a μ-dioxo mode.[11−17]

The gas-phase experiments involving the uranyl cation have proven particularly useful for determining specific reactivity with respect to oxidation state, coordination number, and degree of donation from ligands.[17−22] In a previous report by our group, it was shown that complexes containing the reduced uranyl cation [UO$_2$]$^+$ will bind O$_2$ in the gas phase.[23] The tendency to add O$_2$ to UO$_2^+$ complexes was dependent on the number and identity of associated ligands. For example, no binding of O$_2$ was observed for the bare cation but efficient addition occurred when one or more aco or H$_2$O ligands occupied equatorial coordination sites. The tendency to add O$_2$ appeared to be influenced by the amount of charge donated from ligand(s) to the uranium metal center. Serial dissociation reactions of the [UO$_2$(aco)$_3$(O$_2$)]$^+$ complex also showed an unusual pattern in which initial elimination of neutral acetone was followed by loss of O$_2$, even though there were still σ-donor aco ligands available for elimination. At the time, it was hypothesized that binding of oxygen caused oxidization of the U(V) center to create a U(VI)-superoxide complex, the formation and stability of which was in some way influenced by the number of donor ligands. A subsequent computational study illustrated that binding likely involves formation of a novel two-electron, three-centered bond between [UO$_2$]$^+$ and O$_2^−$, with significant interaction between the uranyl 5fφ and the O$_2$ π*$_{xy}$ orbitals.[24]

In the present study, we investigated the association reactions of H$_2$O and O$_2$ to formally U(V) complexes [UO$_2$(aco)]$^+$ and [UO$_2$(dmso)]$^+$. The aco and dmso species were chosen because the two ligands contain the same number of atoms and hence have the same number of vibrational degrees of freedom (DOF) but differ significantly in their nucleophilicity and gas-phase basicity. Controlling for the number of vibrational DOF was important in this study, as this can influence the rates of gas-phase ligand addition and dissociation reactions by absorbing and accommodating reaction energy. With respect to the σ-donating ligands, the U(V) species tends to behave as a Lewis acid but toward O$_2$ the reactive U(V) complex donates electron density from the metal center to the ligand, thus acting more like a Lewis base. By examining the intrinsic reactivity of
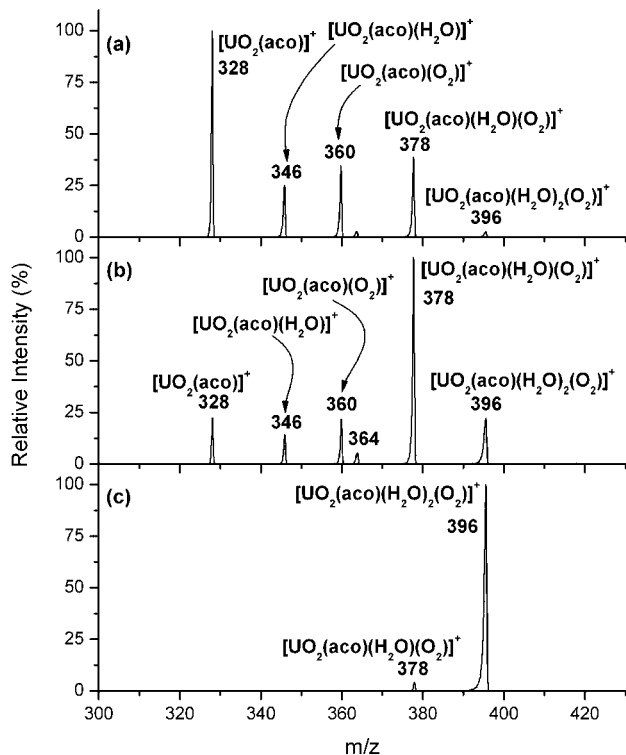
* To whom correspondence should be addressed. E-mail: mike.vanstipdonk@wichita.edu (M.J.V.S.), gary.groenewold@inl.gov (G.S.G.).
† Wichita State University.
‡ California Institute of Technology.
§ Pacific Northwest National Laboratory.
|| Idaho National Laboratory.

Uranyl(V) Dioxocations

J. Phys. Chem. A, Vol. 113, No. 11, 2009 **2351**

Figure 1. Mass spectra of isolated $[UO_2(aco)]^+$ reacting in a mixed atmosphere containing H_2O and O_2 for (a) 10 ms, (b) 100 ms, and (c) 1000 ms.

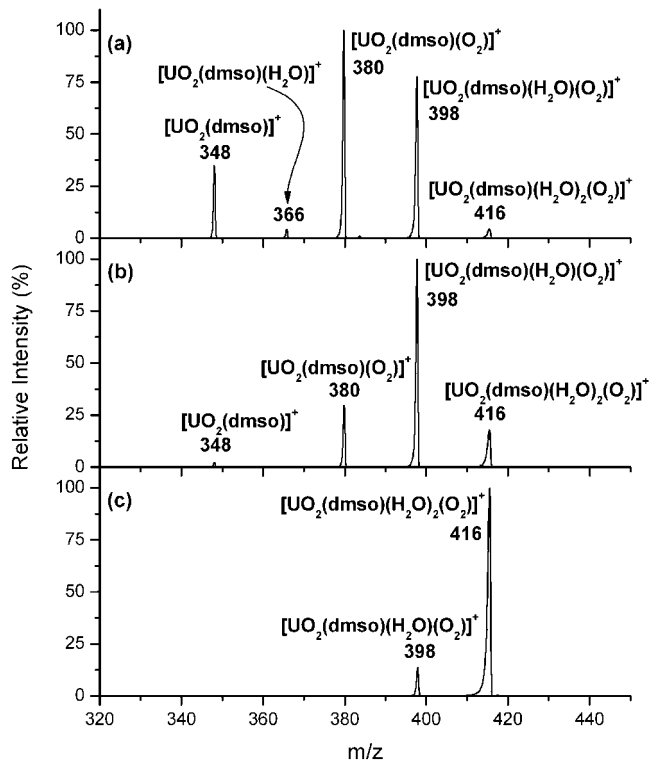**Figure 2.** Mass spectra of isolated $[UO_2(dmso)]^+$ reacting in a mixed atmosphere containing H_2O and O_2 for (a) 10 ms, (b) 100 ms, and (c) 1000 ms.

$[UO_2(aco)]^+$ and $[UO_2(dmso)]^+$, we were able to investigate in a more systematic way the role of σ-donor basicity on the tendency to add either H_2O or O_2 and test the hypothesis that addition of the latter is enhanced by inclusion of strong σ-donors bound to the UO_2^+ center.

Experimental measurements of ligand addition rates, ligand elimination, and ligand exchange were performed using tandem (quadrupole) ion trap mass spectrometry. Precursor aco and dmso-coordinated U(V) dioxocations were generated by ESI. Comprehensive density functional theory calculations were used to predict conformations of relevant species complexes, to determine ligand binding energies, and to predict vibrational features.

Experimental Methods

Electrospray Ionization Mass Spectrometry (ESI-MS). ESI mass spectra were generated using a Finnigan LCQ-Deca ion trap mass spectrometer (ThermoFinnigan, now Thermo Scientific Corp., San Jose CA). In a previous ESI study of O_2 addition to UO_2^+ complexes, we relied upon harsh ESI conditions to cause reduction of uranyl ion. In the present experiments, we enhanced formation of the UO_2^+ complexes by using spray solutions composed in part of UO_2I_2 in deionized H_2O. Because of the disparate ionization energies and electron affinities of UO_2^+ and I^-, collisions in the ion transfer region of the ESI source tend to cause reductive elimination of I from $[UO_2I(aco)_n]^+$ or $[UO_2I(dmso)_n]^+$ to furnish $[UO_2(aco)_n]^+$ or $[UO_2(dmso)_n]^+$, respectively.

The solution of UO_2I_2 was created by dissolving 0.05 g of UO_3 in approximately $1-2$ μL of H_2SO_4 followed by gentle heating for approximately 24 h. The UO_2SO_4 solution thus produced was diluted with 10 mL of deionized H_2O. The UO_2SO_4 solution was added to 10 mL of a 5 mM solution of BaI_2 in deionized H_2O. A combination of the two solutions

caused precipitation of $BaSO_4$, and the resulting aqueous UO_2I_2 solution was separated by decantation. Spray solutions for the ESI experiments were generated by spiking 1 mL of UO_2I_2 solution with 5.00 or 3.00 μL of aco or dmso, respectively. Solutions were infused into the ESI-MS instrument via a syringe pump maintained at a flow rate of $3-5$ $\mu L/min$.

The atmospheric pressure ionization stack settings for the LCQ instrument (lens voltages, quadrupole, octapole voltage offsets, etc.) were optimized for maximum ion transmission to the ion trap mass analyzer using the autotune routine within the LCQ program. The spray needle voltage was maintained at $+5$ kV and the N_2 sheath gas flow at 25 units (arbitrary to the LCQ instrument, corresponding to approximately 0.375 L/min). As in previous studies, the heated capillary was maintained at a relatively high temperature of 200 °C to facilitate elimination of neutral iodine to furnish the $[UO_2(aco)]^+$ and $[UO_2(dmso)]^+$ complexes.[23] The ion trap analyzer was operated at a pressure of $\sim 1.5 \times 10^{-5}$ Torr. A helium bath/buffer gas was used to improve trapping efficiency and functioned as a collision gas for CID experiments.

Ligand addition reactions of H_2O and/or O_2 were monitored by the isolation and storage of aco or dmso ligated UO_2^+ ion in the ion trap. The H_2O is present in the ion trap because of its use as a spray solvent. The O_2 is present in significant partial pressures within the ion trap because ESI is an atmospheric ionization method. Previous investigations have shown that both H_2O and O_2 are present at partial pressures sufficient to produce pseudo-first-order reaction conditions.[23] Addition of O_2 has been confirmed in the past using both He gas seeded with O_2 and ^{18}O labeled gas. Because of the relatively low concentrations of aco and dmso used to make the ESI spray solutions, association reactions to produce aco or dmso adducts were not observed.

The multiple-stage CID and gas-phase association reaction experiments were performed using previously established
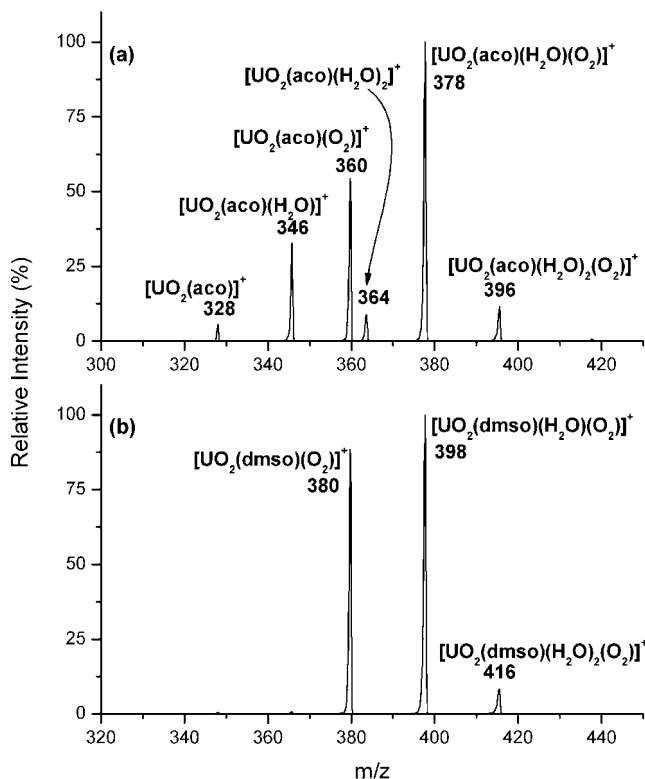
Figure 3. Mass spectra acquired after CID of $[UO_2(lig)(H_2O)(O_2)]^+$ produced from condensation of $[UO_2(lig)]^+$ with O_2 and H_2O, where lig is (a) acetone and (b) dimethylsulfoxide.
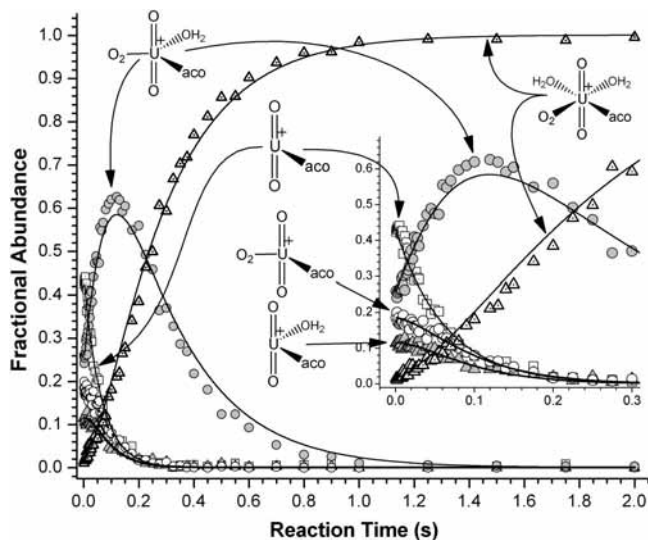
Figure 4. Kinetic profile of association reactions from $[UO_2(aco)]^+$. The inset shows an expanded plot of the kinetic profile for reaction times up to 0.3 s.

procedures.[18−22] Values for the salient instrumental parameters were: a) an isolation width between 1.0 and 3.0, b) an activation Q of 0.300 (used to adjust the q_z value for the resonant excitation of the precursor ion), and c) an activation amplitude ranging of 0−20% (of 5V). The reactant cations (either $[UO_2(aco)]^+$ or $[UO_2(dmso)]^+$ were isolated in the ion trap, where they underwent ligand addition reactions with adventitious H_2O and O_2 that were also present in the ion trap. Ion reaction times were varied from 1 to 5000 ms to observe the temporal variation in the distribution of the product ions. Kinetic plots were generated by measuring ion intensities at discrete time intervals and plotting relative abundance values for each ion as a function
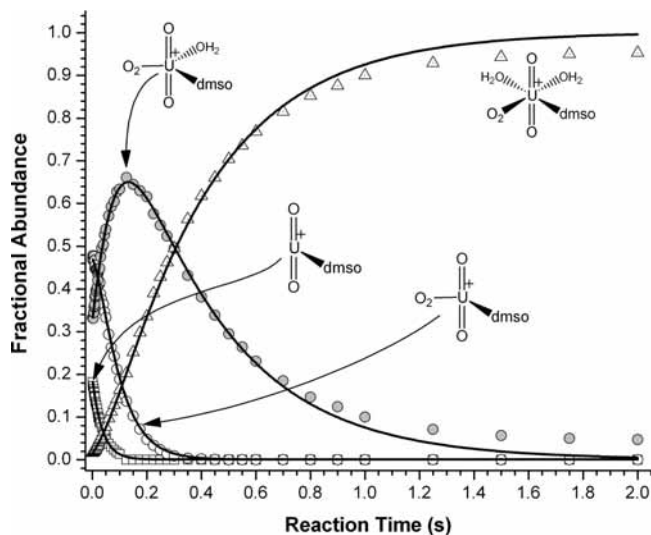

Figure 5. Kinetic profile of association reactions from $[UO_2(dmso)]^+$.

of time. Relative abundance values for reactant and product ions at each reaction time were calculated by dividing the intensity of each individual ion by the total ion intensity. Experimentally determined relative ion intensities are reproducible to better than 20% relative standard deviation.

Kinetic Modeling. Reaction rates were modeled, and rate constants calculated, using the *Berkeley Madonna* software package that utilizes a numerical Runga−Kutta integration algorithm to solve the differential equations based on the reactions of the system.[25] The program uses the downhill simplex method as documented in *Numerical Methods in C* for curve fitting.[26] The model used for this fit was based on a pseudo-first-order approximation of the reactions with respect to the oxygen and water concentrations. The root-mean-square (rms) error was used to measure the degree of deviation of the model from each experimental data point, which was expressed as a percentage of the average ion abundance over the range of time in the experiment. Previous kinetics experiments by our group have shown that rms errors ranging from 1 to 30% provides acceptable agreement between the experiment and model.[23]

Density Functional Theory Calculations. We used the relativistic effective core potential (RECP) density functional theory (DFT) to calculate the geometries, binding energies, and frequencies for complexes containing the U(V) UO_2^+ cation. Our recent work[24] has suggested that the hybrid B3LYP functional[27,28] may be underestimating the binding energy of dioxygen to uranyl(V) systems relative to the binding energy of acetone ligands. In the quest for more accurate computational methods for calculating U(V)−ligand bond dissociation energies, we have tested the newly developed M06-class functionals.[29,30] For the smallest U(VI)−superoxo adduct, $UO_2^+-O_2(\eta^2)$, we also performed coupled-cluster calculations with singles, doubles, and perturbative triples excitations (CCSD(T)).[31−33] Binding energy values calculated using the M06-L local functional (without spin−orbit corrections) provided agreement with the experimental trends (below), and hence the M06-L functional was used for comparative $UO_2^+(lig)$ binding energy calculations in the present study. For comparison purposes, the results obtained with the B3LYP functional are included as Supporting Information in Tables 1S−3S.

The geometries of all complexes were optimized with the standard Stuttgart small-core (SSC) RECP[34] and the correspond-

SCHEME 1: Main Reaction Pathway for the Addition of H$_2$O and/or O$_2$ to [UO$_2$(aco)]$^+$
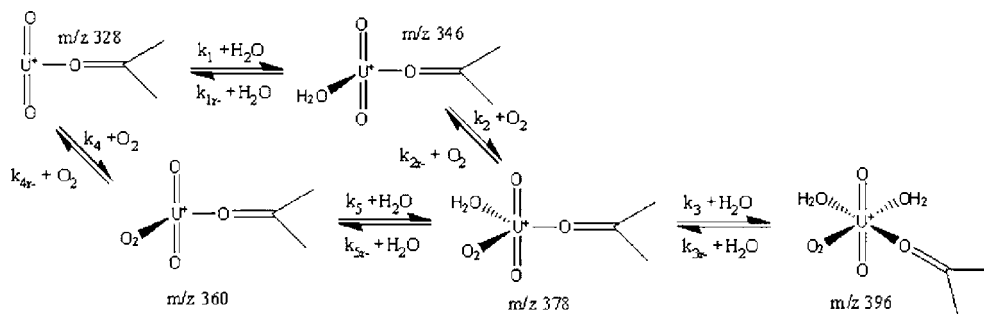
TABLE 1: Forward Rate Constant Values for the Addition of H$_2$O and/or O$_2$ to [UO$_2$(aco)]$^+$

forward reaction	rate constant, k_n	k_n values (cm^3 s^{-1} molecule^{-1})	% efficiency (relative to k_{ADO})
[UO$_2$(aco)]$^+$ + H$_2$O	k_1	6.36×10^{-10}	30
[UO$_2$(aco)(H$_2$O)]$^+$ + O$_2$	k_2	3.74×10^{-10}	69
[UO$_2$(aco)(H$_2$O)(O$_2$)] + H$_2$O	k_3	3.87×10^{-10}	18
[UO$_2$(aco)]$^+$ + O$_2$	k_4	1.39×10^{-10}	26
[UO$_2$(aco)(O$_2$)]$^+$ + H$_2$O	k_5	2.13×10^{-09}	100

ing basis set on U and the standard 6-311G++(d,p) basis set with diffuse functions on the light atoms. In addition, single-point energy calculations were performed using more extended basis sets, namely the SSC basis set augmented with the two g-functions of the Stuttgart large-core basis set on U (SSC(2g)) and the 6-311++G(3df,3pd) basis set on other elements. Control calculations for complexes of UO$_2^+$ with H$_2$O and O$_2$ show (Table 1S of the Supporting Information) that this procedure leads to small differences in binding energies (<0.35 kcal/mol) when compared to results obtained after full optimization at the B3LYP/SSC(3g,1h)/aug-cc-pVTZ level. Full geometry optimization of UO$_2^+$−O$_2$(η^2) was also performed at the CCSD(T)/SSC(2g)/6-311++G(3df,3dp) level, including all electrons in the correlation treatment.

Electronic structure calculations were performed with the *NWChem* program package[35] and were based on the unrestricted formalism. Vibrational frequencies were computed numerically at the B3LYP/SSC/6-311++G** level. The standard Gibbs free energy of each species in the gas phase was calculated using the standard rigid rotor-harmonic oscillator approximation without scaling.

Results and Discussion

Gas-Phase Addition Reactions of H$_2$O and O$_2$ to [UO$_2$(aco)]$^+$ and [UO$_2$(aco)]$^+$. Competitive addition reactions of H$_2$O and O$_2$ to [UO$_2$(aco)]$^+$ were conducted by selectively isolating the relevant precursor ion using a notched rf waveform. It is important to note that in these experiments only the ion selected, in this case [UO$_2$(aco)]$^+$, is stored in the ion trap and all other potential reacting species are resonantly ejected from the ion trap prior to the imposed reaction period. Figure 1 shows the temporal evolution of the product ions in spectra generated by the isolation and storage, without imposed collisional activation, of [UO$_2$(aco)]$^+$ for 10 ms (1a), 100 ms (1b), and 1000 ms (1c). The appearance of product ions with *m/z* values higher than that of the precursor ion signals formation of adducts by ion−molecule association reactions that occur during the imposed isolation/storage time.

After 10 ms reaction time (part a of Figure 1), the base peak in the product ion spectrum was unreacted [UO$_2$(aco)]$^+$ precursor at *m/z* 328. The most abundant adduct ion at this time was

the heterogeneous binary species [UO$_2$(aco)(H$_2$O)(O$_2$)]$^+$ at a *m/z* of 378. Ions at *m/z* 346 and 360, formed by addition of a single H$_2$O or O$_2$ molecule respectively, were present at lower relative abundance as was a small peak *m/z* of 396 that corresponds to [UO$_2$(aco)(H$_2$O)$_2$(O$_2$)]$^+$. [UO$_2$(aco)(H$_2$O)(O$_2$)]$^+$ became the base peak at 100 ms reaction time (part b of Figure 1), and the intensity of the [UO$_2$(aco)(H$_2$O)$_2$(O$_2$)]$^+$ ion increased to ca. 25%. At the longest reaction time (1000 ms, part c of Figure 1), the base peak was [UO$_2$(aco)(H$_2$O)$_2$(O$_2$)]$^+$ at *m/z* of 396. No further addition of either H$_2$O or O$_2$ was observed for reaction times extended out to 5000 ms, suggesting the *m/z* 396 ion represents a UO$_2^+$ complex for which all equatorial coordination sites are occupied. Note also that addition of a second O$_2$ to the [UO$_2$]$^+$ complexes was not observed, which is consistent with the notion that O$_2$ addition is a redox process that cannot occur once uranium has been converted to the VI oxidation state.[23] The reactivity exhibited by [UO$_2$(aco)]$^+$ in the present study is fully consistent with earlier investigations of related UO$_2^+$ complexes by our group.[23]

Figure 2 shows the corresponding product ion spectra generated by isolation and reaction of [UO$_2$(dmso)]$^+$ for 10 ms (2a), 100 ms (2b), and 1000 ms (2c). The experiments with [UO$_2$(dmso)]$^+$ were run directly after those with [UO$_2$(aco)]$^+$ to ensure that both species experienced the same (gas phase) reaction conditions. After 10 ms reaction time (part a of Figure 2), the base ion in the mass spectrum corresponds to formation of [UO$_2$(dmso)(O$_2$)]$^+$ at *m/z* of 380. Direct addition of O$_2$ appears to be favored for [UO$_2$(dmso)]$^+$ over [UO$_2$(aco)]$^+$ and is especially apparent when the relative intensities of [UO$_2$(lig)(O$_2$)]$^+$ and [UO$_2$(lig)(H$_2$O)]$^+$ are compared for the aco and dmso precursor ions. The nearly exclusive addition of O$_2$ to [UO$_2$(dmso)]$^+$ is consistent with the hypothesis that the basicity of the σ-donor ligand significantly influences the tendency to add O$_2$. Other ions observed after the imposed 10 ms reaction time include those formed by addition of H$_2$O, (O$_2$ and H$_2$O), and (O$_2$ and 2 H$_2$O) at *m/z* values of 366, 398, and 416, respectively. After a reaction time of 100 ms (part b of Figure 2), the [UO$_2$(dmso)]$^+$ precursor ion was depleted to less than 5% relative intensity, and the base peak in the spectrum was the heterogeneous binary adduct, [UO$_2$(dmso)(H$_2$O)(O$_2$)]$^+$, at *m/z* 398. The dominant peak observed after 1000 msec reaction time (part c of Figure 2) was [UO$_2$(dmso)(H$_2$O)$_2$(O$_2$)]$^+$ at *m/z* of 416, and no further addition of either H$_2$O or O$_2$ ligands was observed for extended reaction times. This was directly analogous to the final product formed from [UO$_2$(aco)]$^+$ by association reactions.

Comparison of ion dissociation patterns also clearly showed stronger O$_2$ binding by the dmso-containing complex. Figure 3 shows CID spectra derived from [UO$_2$(lig)(H$_2$O)(O$_2$)]$^+$, which was initially formed by condensation of [UO$_2$(lig)]$^+$ with O$_2$ and H$_2$O for lig = aco (3a) and dmso (3b), respectively. For

SCHEME 2: Main Reaction Pathway for the Addition of H₂O and/or O₂ to [UO₂(dmso)]⁺
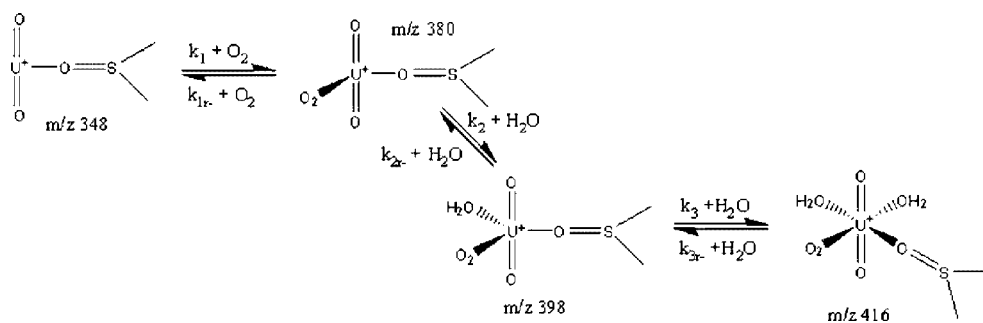
TABLE 2: Forward Rate Constant Values for the Addition of H₂O and/or O₂ to [UO₂(dmso)]⁺

forward reaction	rate constant, k_n	k_n values $(cm^3 \, s^{-1}$ molecule$^{-1})$	% efficiency (relative to k_{ADO})
[UO₂(dmso)]⁺ + O₂	k_1	4.12×10^{-10}	76
[UO₂(dmso)(O₂)]⁺ + H₂O	k_2	1.30×10^{-09}	61
[UO₂(dmso)(H₂O)(O₂)]⁺ + H₂O	k_3	2.63×10^{-10}	12

TABLE 3: Electronic Binding Energies (ΔE_e) and Bond Distances for the Uranyl(V) Superoxo Complex UO₂⁺O₂(η^2) Calculated with CCSD(T) and Several Density Functional Theory (DFT) Methods[a]

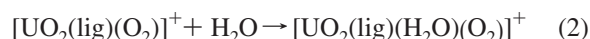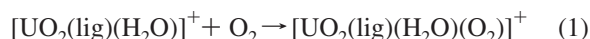| method	ΔE_e, kJ/mol	U=O, Å	U···O, Å	O−O, Å
M06	−63.4	1.756	2.302	1.294
B3LYP[b]	−81.3	1.738	2.293	1.290
M06-L	−101.7	1.735	2.334	1.275
PBE[b]	−143.2	1.756	2.304	1.294
PW91[b]	−145.5	1.756	2.302	1.294
CCSD(T)[c]	−154.2	1.751	2.224	1.314
LDA[b]	−222.3	1.741	2.256	1.276

[a] Optimized with the SSC/6-311++G** basis set followed by single point energy calculations with the SSC(2g)/6-311++G-(3df,3dp) basis set. [b] Ref 24. [c] Optimized with the SSC(2g)/6-311++G(3df,3dp) basis set.

these experiments, the respective binary adduct ions were first synthesized from [UO₂(lig)]⁺ using ion−molecule association reactions, then isolated, and finally dissociated using collisional activation. For both the aco and dmso-containing complexes, the precursor ion remained the base peak in the CID spectrum, a result we attribute to rapid association reactions that the fragmentation products participate in on the time scale of this experiment. However, despite the influence on ion intensity distributions by the association reactions, it is clear from the spectrum in part a of Figure 3 that CID of [UO₂(aco)(H₂O)(O₂)]⁺ generated [UO₂(aco)(O₂)]⁺, [UO₂(aco)(H₂O)]⁺, and [UO₂(aco)]⁺ through competitive elimination of H₂O, O₂, or both ligands. The [UO₂(aco)(H₂O)₂]⁺ and [UO₂(aco)(H₂O)(O₂)]⁺ species were generated by H₂O addition reactions to the [UO₂(aco)(O₂)]⁺ and [UO₂(aco)(H₂O)]⁺ fragment ions. A comparison of relative peak intensities shows that loss of H₂O is competitive with loss of O₂, with the former favored by a factor of ∼1.7:1.

For the dmso complex, CID of [UO₂(dmso)(H₂O)(O₂)]⁺ (part b of Figure 3), loss of O₂ is not competitive with the loss of H₂O. [UO₂(dmso)(O₂)]⁺ was produced by exclusive elimination of the H₂O ligand, and the fragment ion accepted one and two H₂O ligands through association reactions to regenerate [UO₂(dmso)(H₂O)(O₂)]⁺ and form [UO₂(dmso)(H₂O)₂(O₂)]⁺. Thus, the comparison of the dissociation spectra shown in Figure 3 reinforces the idea that the precursor ion that contains dmso more effectively binds the O₂ ligand than does the analogous complex with aco, a result consistent with the hypothesis that

O₂ binding is enhanced by the presence of the more basic σ-donor ligand.

The multiple-stage isolation and reaction capabilities of the ion trap also allowed for an examination of displacement reactions for adducts of the [UO₂(aco)]⁺ and [UO₂(dmso)]⁺ cations. For these experiments, the [UO₂(aco)(H₂O)]⁺, [UO₂-(dmso)(H₂O)]⁺, [UO₂(aco)(O₂)]⁺, and [UO₂(dmso)(O₂)]⁺ ions were selectively isolated and allowed to react with H₂O and O₂ in the ion trap for a period of 30 ms. The resulting product ion spectra are provided in Figure S1 of the Supporting Information. General reaction pathways observed included:

$$[UO_2(lig)(H_2O)]^+ + O_2 \rightarrow [UO_2(lig)(H_2O)(O_2)]^+ \quad (1)$$

$$[UO_2(lig)(O_2)]^+ + H_2O \rightarrow [UO_2(lig)(H_2O)(O_2)]^+ \quad (2)$$

$$[UO_2(lig)(H_2O)]^+ + O_2 \rightarrow [UO_2(lig)(O_2)]^+ + H_2O \quad (3)$$

$$[UO_2(lig)(O_2)]^+ + H_2O \rightarrow [UO_2(lig)(H_2O)]^+ + O_2 \quad (4)$$

For all four precursor ions, the dominant product ion had the formula [UO₂(lig)(H₂O)(O₂)]⁺ (reactions 1 and 2) with the species [UO₂(lig)(H₂O)₂(O₂)]⁺ also observed at a relative abundance of ∼10%. [UO₂(lig)(H₂O)]⁺ also reacted via displacement of H₂O by O₂ (reaction 3) in both the acetone and dmso complexes, with the latter complex undergoing this
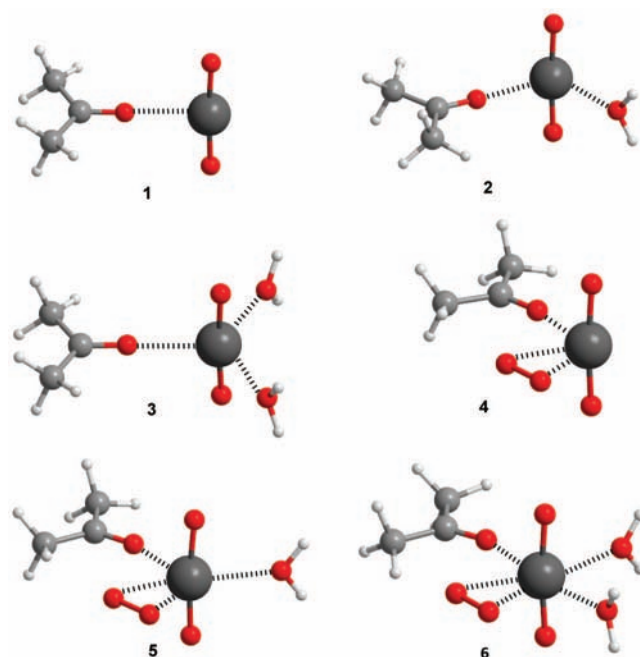
Figure 6. Structures of complexes [UO₂(ACO)(H₂O)₀₋₂]⁺ and [UO₂-(ACO)(H₂O)₀₋₂(O₂)]⁺ optimized at the M06-L/SSC/6-311+G** level of theory.

Uranyl(V) Dioxocations

J. Phys. Chem. A, Vol. 113, No. 11, 2009 **2355**
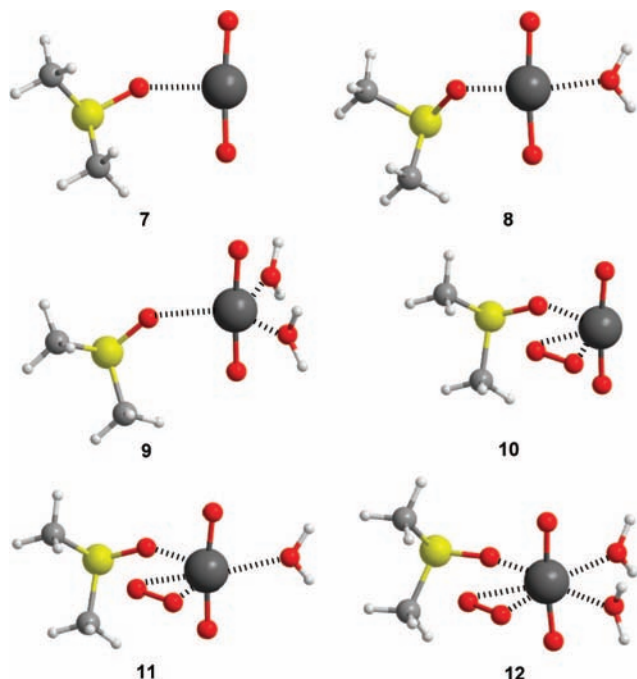
Figure 7. Structures of complexes $[UO_2(DMSO)(H_2O)_{0-2}]^+$ and $[UO_2(DMSO)(H_2O)_{0-2}(O_2)]^+$ optimized at the M06-L/SSC/6-311+G** level of theory.

displacement more readily. Multiple water adduct products were also observed in minor abundance: for acetone $[UO_2(aco)(H_2O)_2]^+$ at *m/z* 364, and for dmso $[UO_2(dmso)(H_2O)_2]^+$ and $[UO_2(dmso)(H_2O)_3]^+$ at *m/z* of 388 and 402, respectively. Most significantly, the displacement of O_2 by H_2O (reaction 4) was observed following isolation and storage of $[UO_2(aco)(O_2)]^+$ in the ion trap (part c of Figure S1 Supporting Information), whereas the same displacement reaction was not observed when the analogous $[UO_2(dmso)(O_2)]^+$ ion was selectively isolated under the same reaction conditions (part d of Figure S1 Supporting Information). The results from study of displacement reactions are therefore consistent with the competitive CID experiments, which suggest that binding and retention of O_2 is enhanced when the more basic σ-donor (dmso) ligand is also bound to the UO_2^+ center.

Experimental Measurements of Gas-Phase Reaction Rates. In the last series of experiments, the rates for ligand addition reactions were measured by systematically altering the isolation/reaction time in the ion trap. Specifically, kinetic plots were generated by isolating $[UO_2(lig)]^+$ in the ion trap from times ranging from 1 to 2000 ms. The fractional abundances (relative to total ion abundance) of the precursor and product ions were measured and plotted as a function of isolation time. Figures 4 and 5 show the kinetic plots generated for the $[UO_2(aco)]^+$ and $[UO_2(dmso)]^+$, respectively. For the $[UO_2(aco)]^+$ system, the $[UO_2(aco)]^+$ reactant species, along with $[UO_2(aco)(H_2O)]^+$ and $[UO_2(aco)(O_2)]^+$ adducts were all observed at an initial isolation/reaction time of 1 ms, and the fractional abundance of each species decreased with increasing reaction time. The relative abundance of $[UO_2(aco)(H_2O)(O_2)]^+$ increased to a maximum at approximately 0.15 s, at which point conversion to $[UO_2(aco)(H_2O)_2(O_2)]^+$ by addition of a second H_2O ligand occurred at longer reaction times. Generation of $[UO_2(aco)(H_2O)_2(O_2)]^+$ was essentially complete by 1 s reaction time. On the basis of the experimental kinetic profiles of the reactant and product ions, Scheme 1 was generated to function as a kinetic model for system. Experimentally determined rate constants, obtained by

fitting the experimental curves, were compared with those obtained using average dipole orientation theory[36−39] to calculate reaction efficiencies. Table 1 shows the values obtained for the forward rate constants designated in Scheme 1 for reduced $[UO_2(aco)]^+$. Addition of a single ligand, either H_2O or O_2, to $[UO_2(aco)]^+$ occurred at a rate efficiency of 30% and 26% respectively, as kinetically modeled. The subsequent reaction rates that led to the formation of $[UO_2(aco)(H_2O)(O_2)]^+$ were much more efficient with $[UO_2(aco)(H_2O)]^+$ adding O_2 and $[UO_2(aco)(O_2)]^+$ adding H_2O at 69% and 100% of the theoretical rate constants, respectively. The reaction rate corresponding to hydration of $[UO_2(aco)(H_2O)(O_2)]^+$ was the least efficient of all of the reactions, consistent with prior studies that showed that, as the uranyl coordination sphere filled, condensation efficiencies decreased.[40]

Figure 5 is the kinetic plot for the isolation of $[UO_2(dmso)]^+$, and pathways outlined in Scheme 2 were used as a model for the system. The reactions observed for $[UO_2(dmso)]^+$ were less complex compared to the analogous acetone system due to the lack of a water adduct to the parent species. This system was modeled as three subsequent reactions; the first was the addition of O_2 followed by two water addition reactions, and Table 2 shows the experimentally determined forward rate constants. The reaction rate efficiency for addition of dioxygen to $[UO_2(dmso)]^+$ was 76%, which was significantly higher than the value modeled for addition of O_2 to the aco-containing complex (26%). The stronger σ-donating dmso ligand increases the efficiency of O_2 addition to the reduced uranyl cation. Following the initial addition of dioxygen to $[UO_2(dmso)]^+$, the subsequent water additions are not as efficient compared to the analogous acetone complexes; efficiencies for the addition of the first and second H_2O molecules to $[UO_2(dmso)(O_2)]^+$ were 61% and 12%, respectively. It is evident that the more basic ligand promotes the addition of O_2 while decreasing the propensity of H_2O addition.

Density Functional Theory Calculations. The binding energies of the $UO_2^+-O_2(\eta^2)$ complexes calculated with six density functionals are shown in Table 3. The DFT results are compared with the benchmark estimates at the CCSD(T)/SSC-(2g)/6-311++G(3df,3dp) level. PBE[41] and PW91[42] functionals yield binding energies that are in good agreement with the CCSD(T) calculations. In contrast, the M06-L,[29] M06,[30] and B3LYP[27,28] methods predict binding energies that are, respectively, 52, 73, and 91 kJ/mol lower than the CCSD(T) value, whereas the LDA method gives a binding energy that is 68 kJ/mol stronger.

The prior UO_2^+-dioxygen results[24] utilized B3LYP and were satisfactory for explaining observed binding preferences in $UO_2(aco)_n(O_2)^+$ complexes; however, the energetic difference between aco and O_2 elimination was not as great as might have been expected based on the branching ratio measured in the collision-induced dissociation spectrum of the $n = 3$ complex. On the other hand, calculations using the PBE and PW91 functionals generated dioxygen$-U(V)O_2^+$ binding energies that were too high. The M06-L functional, which yields binding energies that are intermediate between values generated using B3LYP and those generated using PBE, provides results qualitatively consistent with the relative binding order indicated by the experiment in the previous[24] and present work.

It should be noted that neither DFT nor CCSD(T) calculations include spin−orbit interactions that are substantial for reaction energies of actinide compounds in variable oxidation states. The spin−orbit contributions lower the energies of open-shell U(V) compounds and thus affect the reaction energies involving

TABLE 4: Changes in Electronic Energies (with and without Zero-Point Energy (ZPE) Corrections) and Standard Gibbs Free Energies (kJ/mol) for Binding of Acetone, Dimethylsulfoxide, Water, and Dioxygen to U(V) Compounds[a]

reaction	lig = aco			lig = dmso		
	ΔE_e	ΔE_e + ZPE	$\Delta G°$	ΔE_e	ΔE_e + ZPE	$\Delta G°$
UO_2^+ + lig	−189.9	−185.0	−141.8	−226.3	−222.4	−187.9
$[UO_2(lig)]^+$ + H_2O	−116.5	−108.6	−81.3	−112.4	−103.0	−65.9
$[UO_2(lig)(H_2O)]^+$ + H_2O	−105.3	−95.4	−57.1	−101.6	−91.8	−54.2
$[UO_2(lig)]^+$ + O_2	−129.0	−122.2	−79.0	−135.6	−129.7	−85.9
$[UO_2(lig)(H_2O)]^+$ + O_2	−137.2	−131.0	−85.6	−144.4	−138.5	−96.5
$[UO_2(lig)(H_2O)_2]^+$ + O_2	−137.0	−131.7	−83.6	−144.6	−139.7	−93.6
$[UO_2(lig)(O_2)]^+$ + H_2O	−124.8	−117.4	−87.9	−121.2	−111.9	−76.4
$[UO_2(lig)(H_2O)(O_2)]^+$ + H_2O	−105.1	−96.1	−55.1	−101.8	−92.9	−51.3

[a] M06-L/SSC(2g)/6-311++G(3df,3dp) single point energies on M06-L/SSC/6-311++G** optimized geometries. Vibrational frequencies were computed at the B3LYP/SSC/6-311++G** level.

TABLE 5: M06-L Optimized Distances[a] **(Angstroms) in 1−12**[a]

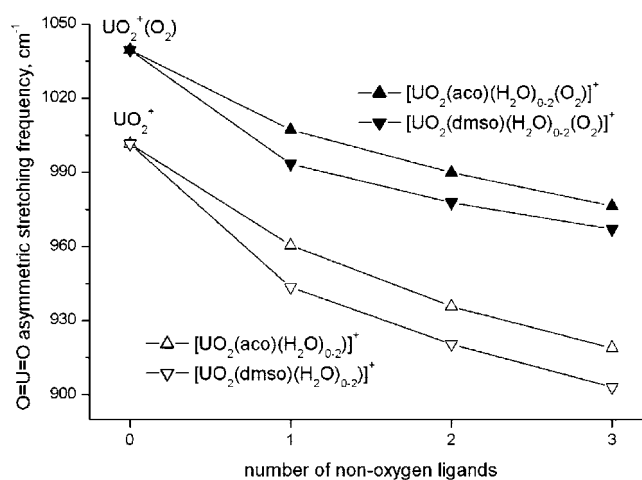| system	U=O	U···aco/dmso	U···H_2O	U···O_2[c]	O−O
1	1.769	2.375			
2	1.780	2.410	2.519		
3	1.782	2.420	2.524		
4	1.749	2.330		2.342, 2.353	1.285
5	1.757	2.364	2.516	2.370, 2.363	1.286
6	1.765	2.410	2.536, 2.529[b]	2.378, 2.381	1.289
7	1.773, 1.780	2.318			
8	1.784, 1.793	2.350	2.526		
9	1.788, 1.800	2.370	2.535, 2.540		
10	1.751, 1.757	2.260		2.348, 2.364	1.288
11	1.759, 1.765	2.291	2.522	2.376, 2.378	1.289
12	1.768, 1.768	2.331	2.539, 2.528[b]	2.387, 2.395	1.292

[a] Obtained with M06-L/SSC/6-311++G**. [b] The H_2O ligand trans to the O_2 ligand. [c] The bond adjacent to the aco/dmso ligand is listed first.
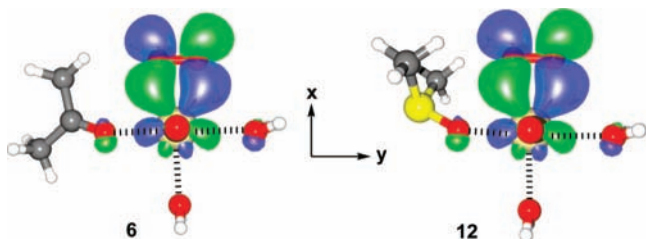
Figure 8. HOMOs (β-spin) for **6** and **12**, showing the strong overlap between the UO_2^+ $5f_\varphi$ and O_2 π^*_{xy} orbitals. MOs are rendered at 0.027 $(e/Å^3)^{1/2}$ isovalues.

Figure 9. Comparison of asymmetric O=U=O stretching frequencies for acetone and dimethylsulfoxide ligated UO_2^+ and $UO_2^+(O_2)$ cations.

U(VI)/U(V) species. The reported spin−orbit contribution for several such reactions from the three independent studies[43−46] ranges from 28.3 to 29.9 kJ/mol. Thus, our best estimate of the $UO_2^+−O_2(\eta^2)$ binding energy at the CCSD(T) level after spin−orbit effects are accounted for is 124.3−125.9 kJ/mol. In what follows, we use the M06-L functional without spin−orbit corrections for modeling this type of uranyl coordination complex, but bear in mind that the better energetic accuracy of M06-L compared to other DFT methods is fortuitous and the inclusion of spin−orbit interactions will likely lead to underestimation of the binding strength of dioxygen to U(V) systems. Aside from systematic differences in the energy of the U(V)−O_2 bond, binding energies and structural parameters calculated with several tested functionals follow similar trends with substitution of aco for dmso and addition of H_2O.

The optimized structures of $[UO_2(aco)]^+$ and $[UO_2(dmso)]^+$ complexes ligated with H_2O and O_2 are shown in Figures 6 and 7. The orientation of the ligands with respect to UO_2^+ is mainly determined by intermolecular repulsions between the uranyl oxygen and ligand lone pairs. Table 4 lists the electronic binding energies (exclusive and inclusive zero-point energy (ZPE) corrections) and standard binding free energies of aco, dmso, H_2O, and O_2 ligands. Table 5 summarizes the optimized distances in all studied complexes **1−12**.

The results confirm that dmso is a stronger oxygen lone-pair donor than aco. The binding of the former donor results in a stronger bond (226.3 kJ/mol for **7** vs 189.9 kJ/mol for **1**) and a shorter intermolecular distance to UO_2^+ (2.318 Å for **7** vs 2.375 Å for **1**). We were also able to find a stable $[UO_2(dmso)]^+$ complex coordinated by sulfur but this was bound by only 96.7 kJ/mol. This is consistent with the hard Lewis acid character of UO_2^+ favoring complexation with hard bases such as oxygen donors.[47]

Water is a weaker electron donor and forms complexes with UO_2^+ that are significantly less stable than those formed with aco and dmso ligands. The stability of $[UO_2(lig)(H_2O)_n]^+$ complexes against H_2O elimination decreases with increasing cluster size and is lower for the more strongly coordinated dmso ligand than for the aco ligand at a fixed cluster size, consistent with expected metal ion complexation behavior. The $UO_2^+···$ H_2O distances closely track the variation in binding energy.

In our earlier communication,[24] we suggested that side-on binding of O_2 to form a superoxo complex is due to favorable overlap between adjacent lobes of the uranyl(V) $5f_\varphi$ and O_2 π^*_{xy} orbitals. Figure 8 illustrates a two-electron, three-centered bonding scheme for coordination of O_2 in **6** and **12**.

In agreement with the previous B3LYP calculations,[24] the addition of electron-donating groups appreciably strengthens the O_2 binding energy despite increasing elongation of the U−O_2

Uranyl(V) Dioxocations

J. Phys. Chem. A, Vol. 113, No. 11, 2009 **2357**

bond. Coordination of a single aco and a single dmso enhances the binding strength by 27.2 and 33.9 kJ/mol, respectively. Addition of the first water to $[UO_2(lig)]^+$ further stabilizes the interaction with O_2 by 8.2−8.8 kJ/mol. Placing the second water in the remaining position trans to O_2 has almost no effect on binding affinity. This suggests that only ligands adjacent to O_2 can directly augment charge transfer in forming the superoxo bond (Figure 8). Indeed, as shown in Figure 8, there is no contribution to the HOMO from the water trans to O_2. Interestingly, this water has a shorter U···OH$_2$ distance than the water adjacent to O_2.

The U=O bond lengths and stretching frequencies can be important indicators of the overall basicity of the uranium center. The calculated U=O bond elongates as the number of equatorial donor ligands increases. Conversely, this bond length markedly decreases (by ∼0.02 Å) upon addition of O_2, which is compatible with an oxidation of the UO_2^+ metal center occurring via formation of the superoxo complex. Similar variations in U=O bond distances were found at the B3LYP level but with absolute values predicted to be ∼0.007 Å longer (Table 3S in the Supporting Information).

The changes in U=O bond lengths are mirrored by changes in O=U=O stretching frequencies. Figure 9 illustrates the expected decrease in the asymmetric uranyl stretching frequencies with increasing the number of donor ligands.[48] The red shift of these vibrational frequencies ($\Delta\nu_a$ = 9−17 cm^{-1}) for the dmso complexes, **7−12**, compared to the corresponding aco complexes, **1−6**, is in accordance with the stronger donor character of dmso.

Calculated changes in standard Gibbs free energies for ligand addition reactions (ΔG°) allow for a direct comparison of the DFT results with experiment (Table 4). Including zero-point energy (ZPE) corrections decreases $\Delta\Delta E_e$ values for the displacement of H_2O by O_2 in $[UO_2(lig)(H_2O)_{1-2}]^+$ complexes, whereas including thermal corrections (T = 298.15 K) has the opposite effect on the $\Delta\Delta G^\circ$ of these reactions. It should be noted that the presence of several low frequency modes (below 100 cm^{-1}) has an adverse effect on the accuracy of the calculations of entropic contributions within the harmonic approximation. Thus, the uncertainty in our assessment of any given ΔG° is not less than 4.2 kJ/mol.

Calculations indicate that $[UO_2(aco)]^+$ exhibits a similar propensity to add H_2O (−81.3 kJ/mol) and O_2 (−79.0 kJ/mol), with the former ligand preferred at high temperatures and the latter ligand preferred at low temperatures. The coordination of a second ligand to form a binary product $[UO_2(aco)(H_2O)(O_2)]^+$ is thermodynamically more favorable for both H_2O (−87.9 kJ/mol) and O_2 (−85.6 kcal/mol). The binding free energy for the subsequent hydration of $[UO_2(aco)(H_2O)(O_2)]^+$ is dramatically reduced (−55.1 kJ/mol). In contrast to $[UO_2(aco)]^+$, $[UO_2(dmso)]^+$ shows a much stronger ability to bind O_2 (−85.9 kJ/mol) than H_2O (−65.9 kJ/mol). Subsequent water addition reactions to form $[UO_2(dmso)(O_2)(H_2O)]^+$ (−76.4 kJ/mol) and $[UO_2(dmso)(O_2)(H_2O)_2]^+$ (−51.3/mol) are thermodynamically less favorable compared to O_2 and the analogous acetone complexes. The predicted binding energy trends are in excellent agreement with the kinetic data and proposed reaction pathways for $[UO_2(aco)]^+$ and $[UO_2(dmso)]^+$ shown in Scheme 1 and Scheme 2.

Conclusions

Using the combination of ESI and tandem ion-trap mass spectrometry the gas-phase reactions of $[UO_2(lig)]^+$ (lig = acetone (aco) or dimethylsulfoxide (dmso)) with H_2O and O_2

were investigated to determine the general effect of ligand charge donation on the reactivity of UO_2^+ with respect to water and dioxygen. The original hypothesis that addition of O_2 is enhanced by strong σ-donor ligands bound to UO_2^+ is supported by results from competitive collision-induced dissociation (CID) experiments, which show near exclusive loss of H_2O from $[UO_2(dmso)(H_2O)(O_2)]^+$, whereas both H_2O and O_2 are eliminated from the corresponding $[UO_2(aco)(H_2O)(O_2)]^+$ species. Ligand-addition reaction rates were investigated by monitoring precursor and product ion intensities as a function of ion storage time in the ion-trap mass spectrometer: these experiments suggest that the association of dioxygen to the UO_2^+ complex is enhanced when the more basic dmso ligand was coordinated to the metal complex. Conversely, addition of H_2O is favored for the analogous complex ion that contains an aco ligand. Experimental rate measurements are supported by density function theory calculations of relative energies, which show stronger bonds between UO_2^+ and O_2 when dmso is the coordinating ligand, whereas bonds to H_2O are stronger for the aco complex.

Supporting Information Available: Tables showing the effect of the basis set size on binding energies, listing electronic binding energies, geometric parameters and frequencies for **1−12** calculated at the B3LYP/SSC/6-311++G** level of theory, and Cartesian coordinates and energies (Hartrees) for the M06-L/SSC/6-311++G** optimized geometries. This material is available free of charge via the Internet at http://pubs.acs.org.

References and Notes

(1) Greenwood, N. N.; Earshaw, A. *Chemistry of the Elements*, 2nd ed.; Butterworth Heinemann: Oxford, Great Britain, 1997; p 1250.

(2) Shulz, W. W.; Navratil, J. D. *Science and Technology of Tributyl Phosphate*; CRC Press: Boca Raton, FL, 1984.

(3) Morse, J. W.; Choppin, G. R. *Rev. Aquatic Sci.* **1991**, *4* (1), 1–22.

(4) Silva, R. J.; Nitsche, H. *Radiochim. Acta* **1995**, *70/71*, 377–396.

(5) Brookins, D. G. *Geochemical Aspects of Radioactive Waste Disposal*; Springer-Verlag: New York, 1984.

(6) Choppin, G. R.; Rizkalla, E. N. *Solution Chemistry of Actinides and Lanthanides. In Handbook on the Physics and Chemistry of Rare Earths*; Gschneider, J. K. A., Eyring, L., Choppin, G. R., Lander, G. H., Eds.; North-Holland: Amsterdam, 1994; Vol. 18, Lanthanides/Actinides: Chemistry, pp 559−590.

(7) Rizkalla, E. N.; Choppin, G. R., *Solution Chemistry of Actinides and Lanthanides. In Handbook on the Physics and Chemistry of Rare Earths*; Gschneider, J. K. A., Eyring, L., Choppin, G. R., Lander, G. H., Eds.; North-Holland: Amsterdam, 1994; Vol. 18,Lanthanides/Actinides: Chemistry, pp 529−558.

(8) Armentrout, P. B.; Beauchamp, J. L. *Chem. Phys.* **1980**, *50* (1), 27−36.

(9) Cornehl, H. H.; Heinemann, C.; Marcalo, J.; deMatos, A. P.; Schwarz, H. *Angew. Chem., Int. Ed. Engl.* **1996**, *35*, 891–894.

(10) Gibson, J. K.; Haire, R. G.; Santos, M.; Marcüalo, J.; Pieres de Matos, A. *J. Phys. Chem. A* **2005**, *109*, 2768–2781.

(11) Kubatko, K.-A. H.; Helean, K. B.; Navrotsky, A.; Burns, P. C. *Science* **2003**, *302*, 1191–1193.

(12) Bhattacharjee, M.; Chaudhuri, M. K.; Purkayastha, R. N. D. *Inorg. Chem.* **1986**, *25*, 2354–2357.

(13) Charpin, P. P.; Folcher, G.; Lance, M.; Vigner, N. E. D. *Acta Crystallogr.* **1985**, *C41*, 1302–1305.

(14) Rose, D.; Chang, Y.-D.; Chen, Q.; Zubleta, J. *Inorg. Chem.* **1994**, *33*, 5167–5168.

(15) Thuery, P.; Masci, B. *Supramol. Chem.* **2003**, *15*, 95–99.

(16) Thuery, P.; Nierlich, M.; Baldwin, B. W.; Komatsuzaki, N.; Hirose, T. *J. Chem. Soc., Dalton Trans.* **1999**, 1047–1048.

(17) Westland, A. D.; Tarafder, M. T. H. *Inorg. Chem.* **1981**, *20*, 3992–3995.

(18) Van Stipdonk, M.; Anbalagan, V.; Chien, W.; Gresham, G.; Groenewold, G.; Hanna, D. *J. Am. Soc. Mass Spectrom.* **2003**, *14*, 1205.

(19) Chien, W.; Anbalagan, V.; Zandler, M.; Hanna, D.; Van Stipdonk, M.; Gresham, G.; Groenewold, G. *J. Am. Soc. Mass Spectrom.* **2004**, *15*, 777.

(20) Groenewold, G. S.; Van Stipdonk, M. J.; Gresham, G. L.; Chien, W.; Bulleigh, K.; Howard, A. *J. Mass Spectrom.* **2004**, *39*, 752.

(21) Van Stipdonk, M. J.; Chien, W.; Angalaban, V.; Bulleigh, K.; Hanna, D.; Groenewold, G. S. *J. Phys. Chem. A* **2004**, *108*, 10448.

(22) Van Stipdonk, M. J.; Chien, W.; Bulleigh, K.; Wu, Q.; Groenewold, G. S. *J. Phys. Chem. A* **2006**, *110*, 959–970.

(23) Groenewold, G. S.; Cossel, K. C.; Gresham, G. L.; Gianotto, A. K.; Appelhans, A. D.; Olson, J. E.; Van Stipdonk, M. J.; Chien, W. *J. Am. Chem. Soc.* **2006**, *128*, 3075–3084.

(24) Bryantsev, V. S.; de Jong, W. A.; Cossel, K. C.; Diallo, M. S.; Goddard III, W. A.; Groenewold, G. S.; Chein, W.; Van Stipdonk, M. J. *J. Phys. Chem. A* **2008**, *112* (26), 5777–5780.

(25) Zahnley, T.; Macey, R.; Oster, G. *Berkeley Madonna*, version 8.0.1; University of California: Berkeley, CA, 2003.

(26) Flowers, B. H. *Numerical Methods in C ++*, 2nd ed.; Oxford University Press: New York, 2000.

(27) Becke, A. D. *Phys. Rev A* **1988**, *38*, 3098.

(28) Lee, C. T.; Yang, W. T.; Parr, R. G. *Phys. Rev. B* **1988**, *37*, 785.

(29) Zhao, Y.; Truhlar, D. G. *J. Chem. Phys.* **2006**, *125*, 194101.

(30) Zhao, Y.; Truhlar, D. G. *Theor. Chem. Acc.* **2008**, *120*, 215.

(31) Purvis, G. D., III.; Bartlett, R. J. *J. Chem. Phys.* **1982**, *76*, 1910.

(32) Raghavachari, K.; Trucks, G. W.; Pople, J. A.; Head-Gordon, M. *Chem. Phys. Lett.* **1989**, *157*, 479.

(33) Watts, J. D.; Gauss, J.; Bartlett, R. J. *J. Chem. Phys.* **1993**, *98*, 8718–8733.

(34) Küsle, W.; Dolg, M.; Stoll, H.; Preuss, H. *J. Chem. Phys.* **1994**, *100*, 7535.

(35) Bylaska, E. J.; de Jong, W. A.; Govind, N.; Kowalski, K.; Straatsma, T. P.; Valiev, M.; Wang, D.; Apra, E.; Windus, T. L.; Hammond, J.; Nichols, P.; Hirata, S.; Hackler, M. T.; Zhao, Y.; Fan, P.-D.; Harrison, R. J.; Dupuis, M.; Smith, D. M. A.; Nieplocha, J.; Tipparaju, V.; Krishnan, M.; Wu, Q.; Van Voorhis, T.; Auer, A. A.; Nooijen, M.; Brown, E.; Cisneros, G.; Fann, G. I.; Fruchtl, H.; Garza, J.; Hirao, K.; Kendall, R.; Nichols, J. A.; Tsemekhman, K.; Wolinski, K.; Anchell, J.; Bernholdt, D.; Borowski, P.; Clark, T.; Clerc, D.; Dachsel, H.; Deegan, M.; Dyall, K.; Elwood, D.; Glendening, E.; Gutowski, M.; Hess, A.; Jaffe, J.; Johnson, B.; Ju, J.; Kobayashi, R.; Kutteh, R.; Lin, Z.; Littlefield, R.; Long, X.; Meng, B.; Nakajima, T.; Niu, S.; Pollack, L.; Rosing, M.; Sandrone, G.; Stave, M.; Taylor, H.; Thomas, G.; van Lenthe, J.; Wong A.; Zhang, Z. *NWChem, A Computational Chemistry Package for Parallel Computers*, Version 5.1; Pacific Northwest National Laboratory: Richland, WA, 2007; pp 99352−0999.

(36) Su, T.; Bowers, M. T. *J. Am. Chem. Soc.* **1973**, *95*, 7609–7610.

(37) Su, T.; Bowers, M. T. *J. Am. Chem. Soc.* **1973**, *95*, 7611–7613.

(38) Su, T.; Bowers, M. T. *Int. J. Mass Spectrom. Ion Phys* **1973**, *12*, 347–356.

(39) Su, T.; Chesnavich, M. J. *J. Chem. Phys.* **1982**, *76*, 5183–5185.

(40) Gresham, G. L.; Gianotto, A. K.; Harrington, P. d.B.; Cao, L.; Scott, J. R.; Olson, J. E.; Appelhans, A. D.; Van Stipdonk, M. J.; Groenewold, G. S. *J. Phys. Chem. A* **2003**, *107*, 8530–8538.

(41) Perdew, J. P.; Burke, K.; Emzerhof, M. *Phys. Rev. Lett.* **1996**, *77*, 3865.

(42) Perdew, J. P.; Wang, Y. *Phys Rev. B* **1992**, *46*, 12947.

(43) Hay, P. J.; Martin, R. L.; Schreckenbach, G. *J. Phys. Chem. A* **2000**, *104*, 6259.

(44) Vallet, V.; Maron, L.; Schimmelpfennig, B.; Leininger, T.; Teichteil, C.; Gropen, O.; Grenthe, I.; Wahlgren, U. *J. Phys. Chem. A* **1999**, *103*, 9285.

(45) Shamov, G. A.; Schreckenbach, G. *J. Phys. Chem. A* **2005**, *109*, 10961.

(46) Tsushima, S.; Wahlgren, U.; Grenthe, I. *J. Phys. Chem. A* **2006**, *110*, 9175.

(47) Cotton, S. *Lanthanide and Actinide Chemistry*; John Wiley & Sons: Chichester, 2006.

(48) Groenewold, G. S.; Gianotto, A. K.; Cossel, K. C.; Van Stipdonk, M. J.; Moore, D. T.; Polfer, N.; Oomens, J.; de Jong, W. A.; Visscher, L. *J. Am. Chem. Soc.* **2006**, *128*, 4802–4813.